Ln(III) complexes as potential phosphors for white LEDs

Akerboom, S.

5 Tuning Eu(III) complexes with dibenzoylmethanates

Seven novel Eu(III)-based coordination compounds with dibenzoylmethanate-type ligands bearing methyl, fluoro, chloro, bromo and iodo substituents on various positions of the phenyl groups have been prepared in yields ranging from 46% to 100%. All compounds have the general formula $HNEt_3[Eu(L)_4]$. In addition, two novel compounds that are described by the general formula $A[Eu(dbm)_4]$ ($A = Li^+$, NBu_4^+) have been synthesized and the structures have been determined using X-ray crystallography. All compounds show bright photoluminescence characteristic of the Eu(III) ion when excited in the ligand-centered absorption band using near-UV radiation. Overall photoluminescence quantum yields range from 13% to 57%, and luminescence lifetimes vary from 0.19 ms to 0.89 ms. The effects of the substituents on the efficiency of the sensitization process have been studied using luminescence lifetime measurements and Judd-Ofelt analysis of the corrected emission spectra. The differences in sensitization efficiency of the ligands can be explained by the different electronic properties of the substituents. The counter ion is found to have a large impact on the luminescent properties of the $[Eu(dbm)_4]^-$ complex ion.

(This Chapter will be published: S. Akerboom, W.T. Fu and E. Bouwman, manuscript in preparation)

5.1 Introduction

Amongst the ligands that are known to efficiently sensitize luminescence of Eu(III) ions, the β-diketones have been the most widely studied class. The early paper by Weissman already concerns the use of *inter alia* benzoylacetonate (bzac), m-nitrobenzoylacetonate and dibenzoylmethanate (dbm) as antenna ligands. In the work that followed, complexes based on β-diketone type ligands were widely investigated [1-5]. Lanthanoid complexes with β-diketones continue to be widely studied as of to date, and have been the subject of an extensive review by Binnemans recently [6]. However, systematic studies on the influence of substituents on dbm molecules on the luminescent properties of the resulting *Ln*(III) complexes appear to be scarce. Systematic investigation to the influence of substitution on the absorption spectra of dibenzoylmethane molecules has been performed in 1955 [7]. In the mid 1960s, Sager *et al.* have investigated the influence of several substituents on the dbm and acac ligands on the luminescence of Eu(III) complexes [2, 3]. More recent systematic investigations on the spectroscopic properties of substituted Hdbm-type molecules mainly focus on their use in sunscreen agents [8-11]. In 2011, the group of Reddy prepared several acetylacetone complexes with highly conjugated substituents, shifting the excitation maximum into the visible part of the spectrum [12]. The aim of this work is to provide a systematic understanding of the photoluminescence properties of the Eu(III) complexes with some novel substituted dibenzoylmethanate ligands. The influence of the substituents on the antenna properties of the ligand is interpreted using the Hammett equation for the electronic properties of the substituents. Judd-Ofelt theory is used to analyze the emission spectra in order to gain more insight in the processes that influence the overall photoluminescence quantum yield of the complexes. Because the photophysical properties of the compounds in the solid state are of interest, the influence of the counter ions should be considered. As was already shown by Mech *et al.*, the counter ions influence the packing of the $[Eu(dbm)_4]^-$ complex ions in the solid state [13]. In turn, this is shown to have a strong impact on the photoluminescent properties of the resulting compounds in. Similar observations were made for tetrakis(naphthoyltrifluoroacetonato)europate(III) complexes with different counter ions [14]. In this chapter, the synthesis of seven Hdbm-type ligands and their Eu(III) complexes is reported; the numbering scheme used throughout this chapter and the composition of the ligands is shown in Figure 5.1. In addition, the photoluminescent properties and structures of two compounds comprising the $[Eu(dbm)_4]^-$ complex ion and a Li^+ or NBu_4^+ cation are compared to assess the influence of the counter ions on the luminescent properties.

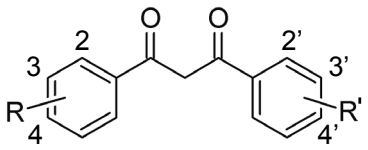

Ligand	R	R'	Complex
H**L1**	4-F	4'-Me	**Eu1**
H**L2**	4-Br	4'-Me	**Eu2**
H**L3**	3-F	4'-Me	**Eu3**
H**L4**	3-Cl	4'-Me	**Eu4**
H**L5**	3-Br	4'-H	**Eu5**
H**L6**	3-I	4'-Me	**Eu6**
H**L7**	2-Cl	4'-Me	**Eu7**

Figure 5.1: An overview of the ligands described in this chapter, showing the numbering scheme used. All complexes are described by the general formula $HNEt_3[Eu(L)_4]$.

5.2 Experimental

5.2.1 General

NMR spectra were recorded on a Bruker DPX-300 spectrometer. Infrared spectra were recorded on a Perkin–Elmer Spectrum Two FTIR spectrometer equipped with the UATR Two accessory. Elemental analysis for C, H, N was performed on a Perkin–Elmer 2400 series II analyzer. Excitation and emission spectra were recorded on a Shimadzu RF–5301PC spectrofluoriphotometer equipped with a solid state sample holder and a UV-blocking filter. Photoluminescence quantum yields were recorded on an Avantes AvaSpec-2048 CCD spectrometer connected to a custom-made integrating sphere, based on the AvaSphere 30REFL, using a modification of the absolute method reported by De Mello [15]. A 1000 Watt Xe-discharge lamp and a SPEX monochromator were used as the excitation source. UV-Vis absorption spectra were measured with the same spectrometer, connected to a solid state reflection probe and using an AvaLight DH-S-BAL light source. For determination of luminescence lifetime, an Edinburgh Instruments FLS920 spectrophotometer was used together with a pulsed laser excitation source.

5.2.2 X-ray crystal structure determination

A crystal was selected for the X–ray measurements and mounted to the glass fiber using the oil drop method and data were collected at 173 K on a Nonius Kappa CCD diffractometer (Mo-Kα radiation, graphite monochromator, $\lambda = 0.71073$ Å)[16]. The intensity data were corrected for Lorentz and polarization effects and for absorption. The programs COLLECT, SHELXS–97, SHELXL–97 were used for data reduction, structure solution and structure refinement, respectively [17-19]. The nonhydrogen atoms were refined anisotropically. The H atoms were geometrically fixed and allowed to ride on the attached atoms. For $Li[Eu(dbm)_4]\cdot H_2O$, the H atoms of the water molecules were not located. For $NBu_4[Eu(dbm)_4]$, the measured crystal was pseudo merohedrally twinned and the refinement was made using twin matrix (–1 0 0 0 –1 0 0 0 1) and BASF parameter 0.53767. The carbon chains of the tetrabutylammonium molecule were refined isotropically. The H atoms were geometrically fixed and allowed to ride on the attached atoms.

5.2.3 General procedure for esterification of benzoic acids

A typical procedure for the synthesis of methyl benzoate esters: 10 mmol of the substituted benzoic acid was converted to the methyl ester by refluxing overnight in 50 mL of absolute methanol in the presence of 1 mL of concentrated sulfuric acid. The resulting mixture was concentrated *in vacuo*, and the resulting oil was dissolved in 50 mL of diethyl ether. The ether solution was transferred to a separatory funnel and washed with saturated sodium hydrogen carbonate (2 × 50 mL) solution and with 30 mL of brine. The combined aqueous layers were extracted with a single portion of 50 mL diethyl ether and the extract was added to the other ether solution. The combined organic layers were dried over magnesium sulfate and concentrated *in vacuo* to give the methyl ester as an oil or solid.

5.2.4 General procedure for the synthesis of dibenzoylmethanates

To a flame dried reflux setup under Ar was added NaH (0.44 g, 11 mmol of a 60% w/w suspension in mineral oil), which was washed with 20 mL of petroleum ether. This was suspended in 50 mL of dry toluene, and the substituted methyl benzoate (10 mmol) was added. To the resulting suspension, a solution of the substituted acetophenone (10 mmol) was added dropwise under stirring. After completing the addition, the mixture was brought to a reflux and left to react overnight. After cooling down to room temperature, the mixture was concentrated *in vacuo* and the resulting residue was taken up in 50 mL of water and acidified to pH ~ 6 using a 1 M solution of HCl. The resulting solution was extracted with ethyl acetate (2 × 50 mL), and the combined organic layers were dried over $MgSO_4$ and concentrated. The residue was recrystallized from hot hexane-ethanol mixtures to yield yellow microcrystalline product. Typically, more product could be obtained by further cooling the mother liquor.

*1-(4-fluorophenyl)-3-(4-methylphenyl)propane-1,3-dione (H**L1**)*

Starting from methyl (4-fluorobenzoate) and 4-methylacetophenone; yield 0.83 g, 32% of a yellow microcrystalline powder. ^{1}H NMR (300 MHz, $CDCl_3$): δ 8.01 (dd, J = 8.9, 5.3 Hz, 1H), 7.92 – 7.85 (m, 2H), 7.33 – 7.27 (m, 2H), 7.17 (dd, J = 8.9, 8.3 Hz, 1H), 6.78 (s, 1H), 2.44 (s, 3H). IR (ν/cm^{-1}): 3073(w), 3031(w), 2916(w), 2859(w), 1599(s), 1531(s), 1492(s), 1400(w), 1378(w), 1297(s), 1219(s), 1185(s), 1155(s), 1123(m), 1104(m), 1086(w), 1054(m), 1011(m), 967(w), 918(w), 847(s), 836(s), 779(vs), 740(m), 695(w), 666(w), 638(w), 632(w), 611(m), 566(m), 506(s), 495(s), 464(m).

*1-(4-bromophenyl)-3-(4-methylphenyl)propane-1,3-dione (H**L2**)*

Starting from 19 mmol methyl (4-methylbenzoate) and 19 mmol 4-bromoacetophenone; yield 0.64 g, 11% of a yellow microcrystalline powder. ^{1}H NMR (300 MHz, $CDCl_3$): δ 7.92 – 7.82 (m, 4H), 7.66 – 7.59 (m, 2H), 7.33 – 7.27 (m, 2H), 6.79 (s, 1H), 2.44 (s, 3H). IR (ν/cm^{-1}): 3028(vw), 2963(vw), 1581(m), 1516(m), 1479(m), 1295(m), 1277(m), 1225(m), 1207(m), 1006(m), 968(m), 916(m), 841(s), 694(m), 663(w), 542(m), 492(s), 468(s).

*1-(3-fluorophenyl)-3-(4-methylphenyl)propane-1,3-dione (H**L3**)*

Starting from methyl (3-fluorobenzoate) and 4-methylacetophenone; yield 1.1 g, 42% of a yellow microcrystalline powder. ^{1}H NMR (300 MHz, $CDCl_3$): δ 7.91 – 7.88 (m, 2H), 7.78 – 7.73 (m, 1H), 7.70 – 7.65 (m, 1H), 7.50 – 7.42 (m, 1H), 7.32 – 7.29 (m, 1H), 7.28 – 7.21 (m, 1H), 6.80 (s, 1H), 2.44 (s, 3H). IR (ν/cm^{-1}): 3075(w), 2988(w), 1685(w), 1610(m), 1526(m), 1504(m), 1474(m), 1440(m), 1302(m), 1246(s), 1210(w), 1179(s), 1123(w), 1076(w), 1057(w), 1017(w), 1000(w), 978(w), 936(w), 909(m), 884(w), 847(w), 829(w), 800(w), 769(vs), 735(s), 684(w), 666(m), 649(w), 577(m), 534(m), 498(m), 460(m).

*1-(3-chlorophenyl)-3-(4-methylphenyl)propane-1,3-dione (H**L4**)*

Starting from methyl (3-chlorobenzoate) and 4-methylacetophenone; yield 0.11 g, 4% of a yellow microcrystalline powder after 3 recrystallisations from hexane-ethanol. ^{1}H NMR (300 MHz, $CDCl_3$): δ 7.95 (t, J = 1.9 Hz, 1H), δ 7.90 (d, J = 8.3 Hz, 2H), δ 7.86 (dt, J = 7.5 Hz, 1.5 Hz, 1H), δ 7.52 (m, J = 8.1 Hz, 1.2 Hz 1H), δ 7.43 (t, J = 8.1 Hz, 1H), δ 7.31 (d, J = 8.1 Hz, 2H), δ 6.79 (s, 1H), 2.44 (s, 3H).

*1-(3-bromophenyl)-3-phenylpropane-1,3-dione (H**L5**)*

Starting from methyl (3-bromobenzoate) and acetophenone; yield 0.93 g, 30% of a yellow microcrystalline powder. ^{1}H NMR (300 MHz, $CDCl_3$): δ 8.12 (t, J = 1.8 Hz, 1H), 8.02 – 7.97 (m, 2H), 7.93 – 7.87 (m, 1H), 7.71 – 7.66 (m, 1H), 7.62 – 7.46 (m, 3H), 8.12 (t, J = 7.9 Hz, 1H). IR (ν/cm^{-1}): 1591(w), 1513(m), 1485(m), 1454(m), 1290(m), 1264(w), 1222(s), 1175(m), 1160(w), 1100(w), 1054(m), 1022(w), 998(w), 911(w), 892(w), 794(w), 757(vs), 704(w), 691(m), 679(s), 655(s), 607(s), 504(w), 451(w).

*1-(3-iodophenyl)-3-(4-methylphenyl)propane-1,3-dione (H**L6**)*

Starting from methyl (3-iodobenzoate) and 4-methylacetophenone; yield 2.13 g, 59% of a yellow microcrystalline powder. ^{1}H NMR (300 MHz, $CDCl_3$): δ 8.21 – 8.29 (m, 1H), 7.95 – 7.85 (m, 4H), 7.32 – 7.25 (m, 2H), 7.23 – 7.20 (d, J = 7.9 Hz, 1H), 6.77 (s, 1H), 2.44 (s, 3H). IR (ν/cm^{-1}): 3065(w), 2996(w), 2950(w), 1711(vs), 1589(w), 1564(m), 1472(w), 1436(s), 1411(m), 1370(w), 1329(w), 1293(s), 1278(s), 1254(vs), 1193(m), 1120(s), 1098(m), 1080(m), 1060(m), 996(m), 963(m), 925(w), 890(m), 839(w), 811(m), 738(vs), 708(vs), 670(s), 645(m), 478(m).

*1-(2-chlorophenyl)-3-(4-methylphenyl)propane-1,3-dione (H**L7**)*

Starting from methyl (2-chlorobenzoate) and 4-methylacetophenone; yield 1.22 g, 45% of a yellow microcrystalline powder. ^{1}H NMR (300 MHz, $CDCl_3$): δ 7.87 – 7.84 (m, 2H), 7.69 – 7.66 (m, 1H), 7.49 – 7.36 (m, 3H), 7.29 – 7.33 (m, 1H), 7.27 – 7.28 (1H), 6.71 (s, 1H), 2.43 (s, 3H). IR (ν/cm^{-1}): 1592(m), 1493(s), 1430(m), 1308(m), 1258(m), 1223(w), 1209(w), 1187(m), 1162(w), 1125(w), 1104(w), 1068(w), 1040(m), 1018(w), 966(w), 830(m), 789(s), 759(vs), 735(s), 712(m), 689(m), 666(w), 638(m), 582(w), 538(w), 468(s).

5.2.5 Complex synthesis

In a typical procedure, 0.5 mmol of the ligand was dissolved in 3 mL of hot ethanol (65 °C) and 0.125 mmol of $EuCl_3 \cdot 6H_2O$ was dissolved in 1 mL of hot ethanol. Then, 0.5 mmol (0.07 mL) of triethylamine was added to the ligand solution and while swirling the resulting solution, the europium solution was added dropwise. The hot mixture was left on the hot plate for 10 minutes, after which it was allowed to cool down to room temperature. The product precipitated as a yellow compound which was collected by filtration, washed with cold ethanol and diethyl ether and dried *in vacuo*. All attempts to grow single crystals of sufficient size for single crystal XRD failed.

*$HNEt_3[Eu(\mathbf{L1})_4]$ (**Eu1**)*

Starting from 0.25 mmol of $EuCl_3$ and 1 mmol of ligand; yield 255 mg, 80% based on Eu, of a light yellow powder. IR (ν/cm^{-1}): 3061(w), 3030(w), 2985(w), 1670(m), 1601(s), 1584(m), 1547(s), 1525(s), 1487(vs), 1418(s), 1380(s), 1295(m), 1219(s), 1207(m), 1180(m), 1154(s), 1128(w), 1114(w), 1093(m), 1056(m), 1013(m), 968(w), 938(w), 886(w), 849(s), 838(m), 774(vs), 741(m), 696(m), 672(w), 638(w), 616(s), 598(m), 582(m), 499(s), 479(s). Elemental analysis calcd (%) for $C_{70}H_{64}EuF_4NO_8$ ($HNEt_3[Eu(\mathbf{L1})_4]$): C 66.35, H 5.09, N 1.11; found: C 65.70, H 4.59, N 1.10.

*$HNEt_3[Eu(\mathbf{L2})_4]$ (**Eu2**)*

Yield 96 mg, 51% based on Eu, of a light yellow powder. IR (ν/cm^{-1}): 1659(w), 1592(m), 1543(m), 1521(s), 1497(m), 1477(m), 1424(s), 1398(m), 1379(m), 1290(m), 1224(w), 1206(w), 1182(w), 1098(w), 1070(m), 1008(s), 951(m), 843(s), 807(w), 769(vs), 722(w), 593(m), 494(m), 469(m). Elemental analysis calcd (%) for $C_{70}H_{64}Br_4EuNO_8$ ($HNEt_3[Eu(\mathbf{L2})_4]$): C 55.36, H 4.25, N 0.92; found: C 55.33, H 3.38, N 0.86.

*$HNEt_3[Eu(\mathbf{L3})_4]$ (**Eu3**)*

Starting from 0.25 mmol of $EuCl_3$ and 1 mmol of ligand; yield 148 mg, 46% based on Eu, of a light yellow powder. IR (ν/cm^{-1}): 1597(m), 1582(m), 1558(s), 1520(s), 1495(s), 1472(s), 1456(s), 1386(m), 1294(w), 1233(m), 1175(m), 1118(w), 952(m), 889(m), 834(w), 800(w), 768(vs), 726(s), 673(w), 561(w), 456(m), 421(m). Elemental analysis calcd (%) for $C_{70}H_{64}EuF_4NO_8$ ($HNEt_3[Eu(\mathbf{L3})_4]$): C 66.35, H 5.09, N 1.11; found: C 65.11, H 4.81, N 1.15.

*$HNEt_3[Eu(\mathbf{L4})_4]$ (**Eu4**)*

Yield 170 mg, 100% based on Eu, of a light yellow powder. IR (ν/cm^{-1}): 3061(w), 3027(w), 2985(w), 1595(s), 1554(s), 1520(s), 1493(s), 1465(s), 1434(m), 1384(m), 1311(w), 1279(m), 1266(m), 1221(m), 1205(m), 1183(m), 1130(w), 1112(w), 1077(w), 1061(m), 1019(w), 942(w), 905(w), 833(w), 790(w), 765(vs), 732(m), 689(s), 672(w), 648(w), 594(w), 544(m), 497(w), 462(s). Elemental analysis calcd (%) for $C_{70}H_{64}Cl_4EuNO_8$ ($HNEt_3[Eu(\mathbf{L4})_4]$): C 62.70, H 4.81, N 1.04; found: C 60.74, H 4.23, N 1.04.

*$HNEt_3[Eu(\mathbf{L5})_4]$ (**Eu5**)*

Yield 120 mg, 66% based on Eu, of a light yellow powder. IR (ν/cm^{-1}): 3061(w), 2985(w), 1731(w), 1704(w), 1671(w), 1592(s), 1573(w), 1547(vs), 1511(vs), 1484(m), 1450(s), 1419(s), 1381(vs), 1304(m), 1282(m), 1266(m), 1214(m), 1178(w), 1127(w), 1059(m), 1024(m), 998(w), 943(w), 900(w), 805(w), 795(w), 750(vs), 704(vs), 686(s), 670(m), 655(s), 638(w), 609(m), 516(m), 467(m). Elemental analysis calcd (%) for $C_{66}H_{60}Br_4EuNO_8$ ($HNEt_3[Eu(\mathbf{L5})_4]$): C 54.19, H 3.86, N 0.96; found: C 52.81, H 3.44, N 0.96.

$HNEt_3[Eu(\mathbf{L6})_4]$ ($HNEt_3[\mathbf{Eu6}]$)

Starting from 0.25 mmol of $EuCl_3$ and 1 mmol of ligand; yield 360 mg, 84% based on Eu, of a light yellow powder. IR (ν/cm^{-1}): 1592(s), 1549(s), 1516(s), 1490(s), 1456(s), 1380(s), 1279(m), 1220(m), 1182(m), 1112(w), 1053(m), 1018(m), 995(w), 940(w), 834(w), 762(vs), 729(m), 668(s), 592(w), 456(m), 418(w). Elemental analysis calcd (%) for $C_{70}H_{64}EuI_4NO_8$ ($HNEt_3[Eu(\mathbf{L6})_4]$): C 49.26, H 3.78, N 0.82; found: C 48.11, H 3.15, N 0.83.

*$HNEt_3[Eu(\mathbf{L7})_4]$ (**Eu7**)*

Yield 130 mg, 78% based on Eu, of a light yellow powder. IR (ν/cm^{-1}): 3057(w), 2980(w), 2605(w), 2498(w), 1672(w), 1591(vs), 1552(s), 1519(s), 1494(s), 1437(vs), 1422(s), 1397(s), 1295(m), 1254(m), 1220(w), 1205(w), 1180(m), 1111(w), 1073(w), 1040(s), 1019(m), 939(w), 834(w), 809(w), 785(m), 754(vs), 737(s), 690(m), 640(m), 595(m), 542(m), 506(m), 453(s). Elemental analysis calcd (%) for $C_{70}H_{64}Cl_4EuNO_8$ ($HNEt_3[Eu(\mathbf{L7})_4]$): C 62.70, H 4.81, N 1.04; found: C 61.07, H 4.70, N 1.36.

*$NBu_4[Eu(dbm)_4]$ (**Eu8**)*

In 5 mL of ethanol was dissolved 2.1 mmol of Hdbm (0.5 g) and 2.1 mmol of NBu_4OH and the mixture was heated to 60 °C. Then, slowly a hot solution of 0.53 mmol of $EuCl_3$ in 5 mL ethanol was added. The mixture was stirred for 15 more minutes and allowed to cool to room temperature, yielding needle shaped crystals. Yield 0.59 g, 86% based on Eu. IR (ν/cm^{-1}): 3351(w, br), 3061(w), 2959(w), 2873(w), 1595(s), 1549(s), 1508(vs), 1463(vs), 1416(vs), 1307(m), 1279(m), 1213(m), 1179(w), 1156(w), 1066(m), 1023(m), 1000(w), 940(w), 925(w), 807(w), 781(m), 738(s), 717(vs), 688(vs), 607(s), 517(m), 502(m). Elemental analysis calcd (%) for $C_{76}H_{84}EuNO_8$ ($NBu_4[Eu(dbm)_4]$): C 70.90, H 6.26, N 1.09; found: C 70.50, H 6.54, N 1.13.

*$Li[Eu(dbm)_4]\cdot H_2O$ (**Eu9**)*

In 5 mL of ethanol was dissolved 0.53 mmol of $EuCl_3\cdot 6H_2O$, and the solution was heated to 60 °C. To another flask with 15 mL of ethanol was added 2.1 mmol of Hdbm (0.5 g), 2.1 mmol of NaOH (90 mg) and 3.75 mmol (0.26 g) of $LiNO_3\cdot 6H_2O$ and heated to 60 °C. The latter solution was added dropwise to the $EuCl_3$ solution with gentle stirring. Upon cooling,

the mixture yielded needle shaped crystals. Yield 0.39 g, 68% based on Eu. IR (ν/cm^{-1}): 3629(w), 3425(w, br), 3058(w), 1594(s), 1547(s), 1509(vs), 1476(s), 1454(s), 1389(s), 1308(m), 1279(m), 1218(m), 1178(w), 1155(w), 1058(m), 1022(m), 999(w), 939(w), 781(w), 744(m), 718(vs), 684(vs), 607(s), 519(s), 502(s).

$HNEt_3[Eu(dbm)_4]$

The synthesis of this compound is described in Chapter 6.

5.3 Results

5.3.1 Synthesis and Characterization

All Hdbm derivatives were synthesized in non-optimized yields following the same basic procedure for Claisen condensation reactions, and were analyzed using IR and NMR spectroscopy. Complex formation was performed by mixing of hot ethanolic solutions of the europium salt and ligand to ensure their complete dissolution and to slow down the precipitation of the product upon addition of the $EuCl_3$ solution. In general it was found that precipitation only starts after nearly complete addition of the $EuCl_3$ solution. The complexes with the substituted dbm ligands all analyze as $HNEt_3[EuL_4]$. The infrared spectra of the compounds are all similar and contain features as expected for these compounds, with aromatic C-H stretching around 3000 cm^{-1}, C=O stretching vibrations around 1590 cm^{-1} and strong bands in the 700-800 cm^{-1} region as a result of out-of-plane bending of the aromatic C-H groups. Unfortunately, all attempts to grow single crystals for structure determination have failed. However, based on the composition, it is assumed that the coordination environment of the Eu(III) ion in these compounds is similar to that of the parent compound, $HNEt_3[Eu(dbm)_4]$ [20-22]. The IR spectra of the two compounds $A[Eu(dbm)_4]$ (A = NBu_4^+ and Li^+) are very similar, the main difference is the absorption at 2873 cm^{-1}, which is characteristic for the NBu_4^+ cation.

5.3.2 X-ray crystal structure

Single crystals of **Eu8**, $NBu_4[Eu(dbm)_4]$ and **Eu9**, $Li[Eu(dbm)_4]\cdot H_2O$, were obtained by direct crystallization from the reaction mixture. Their crystal structures were determined using single crystal X-ray diffraction. Crystallographic data for of **Eu8** and **Eu9** are given in Table 5.1 and some selected bond distances and angles are listed in Table 5.2. Both compounds crystallize in the monoclinic *C*2/*c* space group. However, the structure of **Eu9** has a single crystallographically independent Eu(III) site, whereas **Eu8** has three, referred to as Eu-a, Eu-b and Eu-c hereafter. Furthermore, in **Eu9** a twofold rotation axis passes through the Eu(III) ion, and as a result there are just four independent Eu-O distances in this complex. In **Eu8**, a twofold rotation axis passes through the center of Eu-b and Eu-c, while the Eu-a site is surrounded by four crystallographically independent ligands. Because the coordination geometry of the Eu(III) sites in **Eu8** resemble each other, the data for only one

site are given in Table 5.2. In both **Eu8** and **Eu9**, the Eu(III) ion is surrounded by four dbm^- ligands binding in a bidentate mode and the geometry of $[Eu(dbm)_4]^-$ complex ion is best described as a distorted square antiprism, as shown in Figure 5.2. For **Eu9**, the Eu-O bond lengths range from 2.352(5) to 2.390(6) Å, for **Eu8** they range from 2.34(1) to 2.428(7) Å, which is normal for this type of bonds [23]. It should be noted that the packing in the structures of **Eu8** and **Eu9** differs substantially. In the latter structure, the alkyl groups of the tetrabutylammonium ions occupy the interspace between two of the ligands coordinated to Eu(III). In **Eu9**, the Li^+ ion resides in the cavities between the complexes and the molecule of water is coordinated to the Li^+ ion.

Table 5.1: Crystallographic data for compounds Eu8 and Eu9.

	Eu8	**Eu9**
formula	$C_{304}H_{326}Eu_4N_4O_{32}$	$C_{60}H_{44}EuLiO_9$
fw	5155.53	2139.74
crystal size [mm^3]	0.10 × 0.25 × 0.25	0.20 × 0.20 × 0.30
crystal color	colorless	colorless
crystal system	monoclinic	monoclinic
space group	*C*2/*c* (no. 15)	*C*2/*c* (no. 15)
a [Å]	28.220(4)	27.348(2)
b [Å]	42.970(6)	8.535(1)
c [Å]	21.415(4)	24.994(2)
α [°]	90	90
β [°]	90.05(3)	108.70(2)
γ [°]	90	90
V [$Å^3$]	25968(7)	5526.0(11)
Z	4	2
d_{calc} [g/cm^3]	1.319	1.284
μ [mm^{-1}]	1.023	1.188
refl. measured / unique	166900 / 22949	27693 / 4760
parameters / restraints	1392 / 18	339 / 24
R1/wR2 [I>2σ(I)]	0.0833 / 0.1177	0.0678 / 0.1828
R1/wR2 [all refl.]	0.1791 / 0.1327	0.0835 / 0.2033
S	1.63	1.09
$\rho_{min/max}$ [$e/Å^3$]	–1.49 / 2.24	–1.44 / 2.02

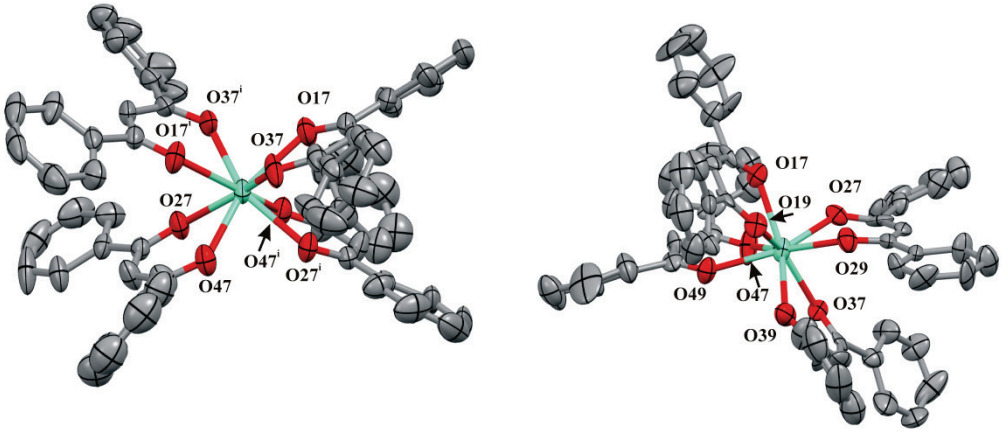

*Figure 5.2: Thermal ellipsoid plot (50% probability contours) of the $[Eu(dbm)_4]^-$ complex ions in **Eu9** ($Li[Eu(dbm)_4]$, left) and one of the three complex ions in **Eu8** ($NBu_4[Eu(dbm)_4]$, right). In both cases, the geometry resembles a distorted square antiprism. Hydrogen atoms have been omitted for clarity and the numbering scheme for O atoms is indicated.*

Table 5.2: Selected bond distances and angles for Eu8 and Eu9.

	Eu8	**Eu9**	
Bond distance (Å)			
Eu1–O17	2.390(8)	Eu1–O17	2.375(5)
Eu1–O27	2.399(9)	Eu1–O27	2.352(5)
Eu1–O37	2.428(7)	Eu1–O37	2.390(6)
Eu1–O47	2.34(1)	Eu1–O47	2.385(5)
Eu1–O19	2.388(9)		
Eu1–O29	2.352(9)		
Eu1–O39	2.41(1)		
Eu1–O49	2.368(8)		
Bond angle (°)			
O17-Eu1-O19	70.2(3)	O17-Eu1-O37	71.8(2)
O27-Eu1-O29	69.2(3)	O27-Eu1-O47	71.1(2)
O37-Eu1-O39	68.6(3)	O27-Eu1-O37	74.0(2)
O47-Eu1-O49	68.8(3)	O17-Eu1-O47	74.5(2)
O17-Eu1-O47	75.6(3)		
O19-Eu1-O49	74.1(3)		
O27-Eu1-O37	75.5(3)		
O29-Eu1-O39	76.7(3)		

5.3.3 Luminescent properties and lifetime

The solid state photoluminescence spectra recorded at room temperature for **Eu1 - Eu9** are shown in Figure 5.3. Excitation spectra were obtained by constantly monitoring the intensity of the Eu(III) $^5D_0 \rightarrow {}^7F_2$ hypersensitive transition at 614 nm while scanning the excitation wavelength. All complexes show two broad excitation bands in the UV and near-

UV (400 nm) region as a result of ligand-centered excitation [3, 4]. With the exception of **Eu7**, the excitation band in the UV region, around 290 nm, is slightly more intense than the second band at 400 nm. These bands also appear in the solid state UV-Vis absorption spectra that are shown in Figure 5.4. The emission spectra obtained by ligand-centered excitation all show lines at 595, 614, 650 and 720 nm. These are characteristic for the Eu(III) ion as a result of transitions from the $^5D_0$ resonance level to the ^7F_J manifold. All emission spectra are dominated by the $^5D_0 \rightarrow {}^7F_2$ transition at 614 nm. Table 5.3 lists the photoluminescence properties for all coordination compounds. The overall quantum yields, upon excitation with 360 nm radiation, range from 13% for **Eu2** to 57% for **Eu8**. The luminescence decay curves measured for **Eu1 - Eu7** could be satisfactorily fitted with a single exponential function, indicating the presence of a single luminescent Eu(III) center in the complexes. Experimental luminescence lifetimes range from 0.19 ms for **Eu2** to 0.89 ms for **Eu7**.

Table 5.3: Photophysical properties of the coordination compounds.

Complex	Φ_{tot} (%)	Ω_2 (10^{-20} cm^2)	Ω_4 (10^{-20} cm^2)	Ω_6 (10^{-20} cm^2)	τ_{exp} (ms)	τ_{rad} (ms)	Φ_{Ln} (%)	η_{sens} (%)
Eu1	24	23.96	2.96	0*	0.31	1.19	26	92
Eu2	13	21.70	2.68	0*	0.19	1.30	15	88
Eu3	27	22.20	4.09	11.47	0.54	1.23	44	62
Eu4	31	21.72	4.85	17.58	0.57	1.22	47	66
Eu5	35	21.53	4.97	20.27	0.55	1.23	45	78
Eu6	22	19.46	4.86	18.91	0.53	1.34	40	54
Eu7	24	9.47	5.73	8.61	0.89	2.18	41	59
Eu8	57	24.03$^{\pm}$	3.87$^{\pm}$	15.76$^{\pm}$	n.d.	1.14$^{\pm}$	n.d.	n.d.
Eu9	42	11.47	3.87	10.77	n.d.	2.18	n.d.	n.d.
$NEt_3[Eu(dbm)_4]$**	27	19.94$^{\pm}$	4.50$^{\pm}$	16.44$^{\pm}$	n.d.	1.32$^{\pm}$	n.d.	n.d.

*Notes: *: $^5D_0 \rightarrow {}^7F_6$ transition was too weak to be observed, **: for comparison, compound reported in Chapter 7; $^{\pm}$: average value for multiple Eu(III) sites ; Φ_{tot} (%): Overall photoluminescence quantum yield at 360 nm excitation, τ_{exp}: experimental lifetime of $^5D_0$ state, Ω_J: Intensity parameters, τ_{rad}: radiative lifetime, Φ_{Ln}: intrinsic quantum yield, η_{sens}: sensitizer efficiency.*

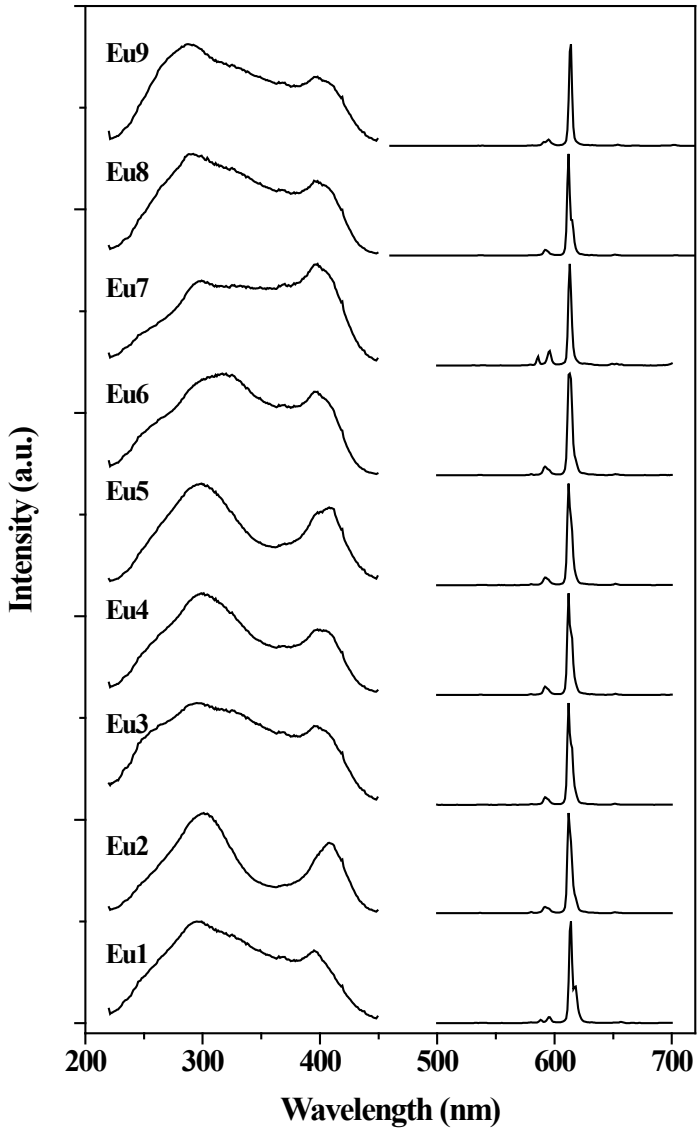

*Figure 5.3: Photoluminescence spectra for **Eu1 - Eu9**. Excitation spectra, shown on the left hand side, are recorded while monitoring the intensity of the strongest emission line at 614 nm. The right hand side shows the emission spectra of the compounds obtained upon excitation at 360 nm. The emission spectra are characteristic for the Eu(III) ion, with lines at 595, 614, 650 and 720 nm, corresponding to the $^5D_0 \rightarrow {}^7F_J$, J =1, 2, 3, 4 transitions.*

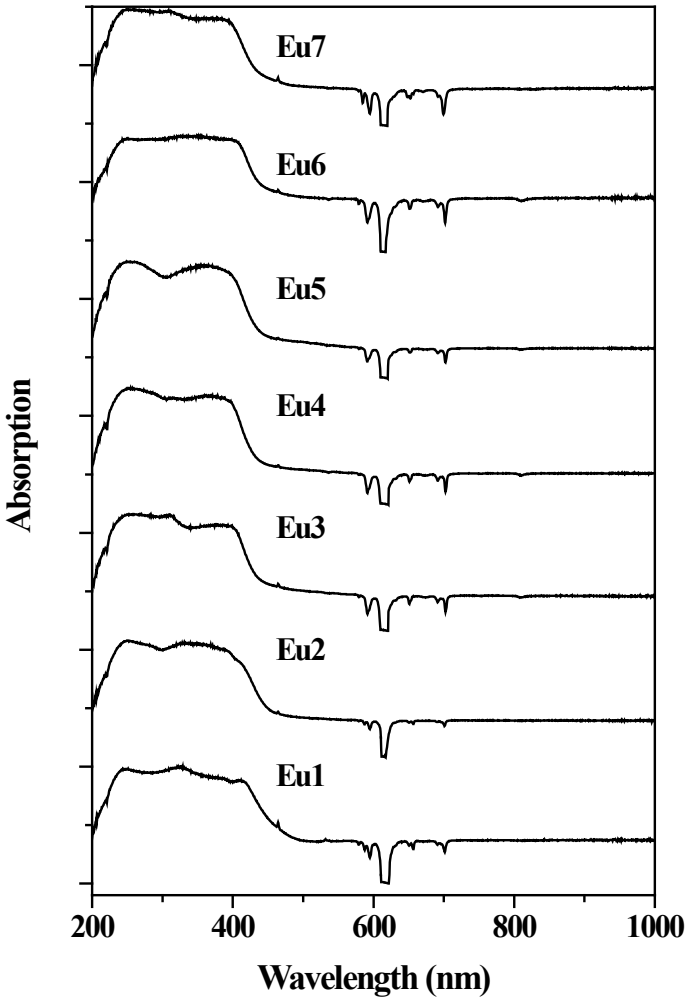

*Figure 5.4: Absorption spectra recorded for the Eu(III) complexes **Eu1** - **Eu7** in the solid state. The downward pointing peaks are due to Eu(III)-centered photoluminescence.*

5.4 Discussion

5.4.1 General remarks on the luminescent properties

The photoluminescence excitation spectra for all complexes show two bands, one centered around 290 nm and 400 nm, respectively. The absorption spectra show similar features and appear to be composed of two broad bands in the UV and nUV region. The emission that results upon excitation in the ligand-centered bands is typical for the Eu(III) ion in a non-centrosymmetric environment. The relatively high intensity of the $^5D_0 \rightarrow {}^7F_2$ electric dipole

(ED) transition with respect to the $^5D_0 \rightarrow {}^7F_1$ magnetic dipole (MD) transition is indicative of a low symmetry coordination site of the Eu(III) ion in all complexes [24].

5.4.2 Influence of the counter ions

The excitation spectra of the compounds with the unsubstituted ligand, $HNEt_3[Eu(dbm)_4]$, **Eu8** and **Eu9**, are highly similar. This is to be expected, because the antenna ligand is the same in all three compounds. However, the counter ion otherwise has a significant influence on the photophysical properties of the $[Eu(dbm)_4]^-$ complex ion. The structure of **Eu8** has three different sites for the Eu(III) ion, while the structure of **Eu9** has just one Eu(III) site. Due to the broad ligand centered absorption bands, it was impossible to selectively excite individual Eu(III) sites in $HNEt_3[Eu(dbm)_4]$ and **Eu8**. In related work, using low temperature spectroscopy, Mech and co-workers have shown that the properties of the various Eu(III) sites can be indeed very different [13]. Thus, only average values could be calculated for the intensity parameters and radiative lifetime, using the overall integrated intensity of the $^5D_0 \rightarrow {}^7F_J$ transitions. The intensity parameters Ω_λ are highly sensitive to the coordination sphere of the Eu(III) ion. From Table 5.3, it can be seen that there are significant differences amongst the three compounds with different counter ions. The observed differences are most likely the result from different packing arrangements of the $[Eu(dbm)_4]^-$ complex ions in those complexes, as different arrangements affect the Eu-O bond distances and angles. Worth noting is the increase in overall quantum yield on going from the $HNEt_3^+$ to Li^+ to NBu_4^+ counter ions, which is most likely due to higher energy transfer efficiency and / or less contributions of non-radiative quenching processes in the latter compounds.

5.4.3 Influence of the substituents

The emission spectra of Eu(III) compounds have been analyzed by using the Judd-Ofelt (JO) theory [25, 26]. According to JO theory, the intensities of a forced electric dipole transition depends only on three parameters (Ω_λ, $\lambda = 2, 4, 6$), which are dependent on the surroundings of the lanthanoid ion. Properties such as the symmetry of the coordination sphere, the nature of the bonds and the basicity of the coordinating atoms are reflected in the parameters [27-31]. The calculated JO parameters for **Eu1 - Eu9** are listed in Table 5.3. All compounds have a high Ω_2, indicating low site symmetry and a relatively covalent bond between Eu(III) and the ligands [32, 33]. Based on the JO parameters, compounds **Eu1**-**Eu7** may be divided into three groups. The first comprises **Eu1** and **Eu2**, and is characterized by $\Omega_2 > 21 \cdot 10^{-20}$ cm^2 and $\Omega_4 < 3 \cdot 10^{-20}$ cm^2. For the compounds in this group the value of the Ω_6 parameter could not be determined because emission of the corresponding $^5D_0 \rightarrow {}^7F_6$ transition was absent. The second group, covering the compounds **Eu3** to **Eu6** has a comparable Ω_2 ($\sim 21 \cdot 10^{-20}$ cm^2) but with $4 \cdot 10^{-20}$ cm$^2 < \Omega_4 < 5 \cdot 10^{-20}$ cm^2. The Ω_6 parameter increases steadily from 11.5 for **Eu3** to 20.3 for **Eu5** and drops slightly to 18.9 for **Eu6**. Compound **Eu7** forms the last 'group' because its JO parameters differ

substantially from all other compounds. The Ω_2 parameter is about half that of all other compounds, while its Ω_4 is the highest of the entire series. The value of the Ω_6 parameter is in between those found for the other two groups. These differences reflect the different coordination environments in the complexes. A large Ω_2 is associated with a highly asymmetric coordination environment and / or covalency of the M-L bonds [31-33]. Its value is similar for the first two groups, indicating a low symmetry coordination sphere and similar nature of the M-O bonds in these compounds. For compound **Eu7** the low Ω_2 suggests substantially different coordination geometry in this compound, as can be expected from the steric demands of the 2-Cl substituent on the ligand. Since the meaning of the Ω_4 parameter is ill-defined it is not appropriate to draw any conclusions from its values [34]. The Ω_6 parameter is linked to the electron density on the donor atoms and to the Coulomb interaction between the lanthanoid ion and the donor atoms [31, 33, 35]. Its value increases when the electron density on the coordinating atoms decreases and when the M-L distance increases or with decreasing covalency [35]. The value of this parameter is negligible in the first group, which indicates a covalent character of the M-O bond. In the second group of compounds, the value of the Ω_6 parameter is fairly large, suggesting a less covalent nature of the M-L bonds compared to the first group. In addition, the trend of Ω_6 for the second group of complexes reflects a decreasing electron density on the ligands on going from **L3** to **L5** and a slight increase for **L6**, which correlates with the electron withdrawing character of the substituent halogen atoms. For the last compound, **Eu7**, Ω_6 takes an intermediate value compared to the other two groups of complexes. This suggests that the nature of the M-L bonds is not as covalent as in **Eu1** and **Eu2**, but more covalent than in **Eu3** - **Eu6**.

5.4.4 Luminescent lifetime and intrinsic quantum yield

The $^5D_0 \rightarrow {}^7F_1$ transition of the Eu(III) ion is of purely MD nature and as such insensitive to the ion's coordination environment. As a result, the radiative lifetime of Eu(III) can be calculated from its emission spectrum, provided that the spectra are corrected for the response of the spectrometer [29]. In that case, the intensity of the MD transition can be used as an internal benchmark and its relaxation (A_{0-1}) rate can be calculated (49 s^{-1}) [29]. The relaxation rate of the other transitions can be found from their intensities I_{0-J} using equation 1.

$$A_{0-J} = A_{0-1}\frac{I_{0-J}}{I_{0-1}} \qquad (1)$$

The total radiative relaxation rate A_{rad} is the sum of all A_{0-J}'s and the radiative lifetime τ_{rad} is the reciprocal of A_{rad}. The radiative lifetimes for **Eu1 - Eu9** have been calculated and are listed in Table 5.3. The excited $^5D_0$ state of Eu(III) is not only depopulated by radiative processes, but also by non-radiative processes such as multiphonon quenching [36]. This is reflected in the experimental lifetime, which is usually shorter than the radiative lifetime. If

the rate of such non-radiative processes is given by A_{nrad}, the sum of A_{rad} and A_{nrad} results in the total relaxation rate A_{tot}, which is in turn the reciprocal of the experimental lifetime τ_{exp}, as shown in equation 2.

$$A_{tot} = \frac{1}{\tau_{exp}} = \frac{1}{\tau_{rad}} + \frac{1}{\tau_{nrad}} \quad (2)$$

The relative contribution of the radiative process to the relaxation of the excited state is known as the intrinsic quantum yield, Φ_{Ln} of the lanthanoid ion [37, 38]. Its value can be calculated from equation 3.

$$\Phi_{Ln} = \frac{A_{rad}}{A_{tot}} = \frac{\tau_{exp}}{\tau_{rad}} \quad (3)$$

The intrinsic quantum yields for **Eu1 - Eu7** are listed in Table 5.3. The lowest value is obtained for **Eu2** at 15%, indicating that the non-radiative processes are mainly responsible for relaxation of the $^5D_0$ state of Eu(III). For the other compounds, the values range from 26% to 47%, which shows that non-radiative decay processes contribute substantially to the depopulation of the Eu(III) $^5D_0$ state in all compounds. As a result, the overall quantum yields are limited.

5.4.5 Antenna efficiency

Using the intrinsic quantum yield and the overall photoluminescence quantum yield Φ_{tot}, the efficiency of the sensitization process η_{sens} can be estimated from the relation $\Phi_{tot} = \eta_{sens} \cdot \Phi_{Ln}$ [37, 39]. The sensitization efficiency is a measure of how effective an antenna the ligand is, and can be used to compare the antenna potential of the ligands. For compounds **Eu1 - Eu7**, the values for sensitization efficiency have been calculated and are listed in Table 5.3. The values range from 54% for **Eu6** to 92% for **Eu1**, indicating moderate to highly efficient ligand-to-metal energy transfer. The sensitization efficiency is determined by the efficiency of the intersystem crossing and ligand to metal energy transfer processes [37]. The efficiency of the energy transfer process depends on the energy gap between the ligand excited triplet state and the accepting level on the lanthanoid ion [40, 41]. In general, the introduction of substituents on the dibenzoylmethane molecule can be expected to affect the following properties:

- The energy levels of the excited singlet and triplet states;
- The intersystem crossing efficiency;
- The orbital overlap between ligand orbitals and metal orbitals.

For ortho-substitution, steric effects may play a role, and in case of meta-substitution, only inductive effects can occur, while both resonance and inductive effects of the substituents

may influence the properties of para-substituted molecules. The excited triplet state of the dbm^- ligands is associated with a double-radical structure resulting from the separation of two electrons of a double bond. Owing to their parallel spin, a strong repulsion exists between these electrons, resulting in the largest possible spatial separation [2]. As a result, the excited triplet state is stabilized by substituents that allow such separation. This stabilizing effect of the ligand T*-state is expected to be the largest for the first group of complexes, consisting of **Eu1** and **Eu2**, with a 4-Me, 4'-F and 4-Me, 4'-Br substitution pattern. Indeed, these compounds show relatively high sensitizer efficiencies around 90%. However, the luminescent centers in these compounds have the lowest intrinsic quantum yields of the series studied, resulting in low overall quantum yields. This indicates that non-radiative processes depopulating the Eu(III) $^5D_0$ state are the limiting factor. Comparison of the compounds **Eu3 - Eu6**, with F, Cl, Br and I as substituents, respectively, shows that the overall quantum yield increases slightly from 27% for **Eu3** to 35% for **Eu5**, and drops to 22% for **Eu6**. The intrinsic quantum yields for all complexes are roughly the same and vary from 40% to 47%. Indeed, the main difference in overall quantum yield is the result from differences in sensitizer efficiency, which show the same trend as the overall quantum efficiency. This can be understood from the ability of the different halogen substituents to lower the energy of the T*-state, that is, the ability to separate the two electrons of the T*-state. The inductive electron-withdrawing power of the halogens increases on going from F to I, lowering the triplet state and thereby facilitating ligand-to-metal energy transfer. This in turn increases sensitizer efficiency. In case of **Eu6**, the ligand T*-state may be too close to the $^5D_0$ level of Eu(III), which allows for thermal assisted back-transfer of energy thus lowering the sensitizer efficiency [41]. Compared to the first group of complexes, the ligands with the halogens on the 3'-position are less efficient antennae.

It has been reported that ortho substitution with F and Cl results in decreased absorption intensity with respect to the unsubstituted dbm molecule, because the conjugation between the benzene ring and the chelate ring is disturbed [11]. Nevertheless, the quantum yield of $HNEt_3$[**Eu7**] with a 2-chloro substituent on the ligand, is still moderate with 24%. This complex has the longest experimental and radiative lifetimes, suggesting that the ligands provide a rigid environment for the luminescent center. Although the coordination sphere around the metal ion may differ substantially from the other complexes, the ability of the ligand $\mathbf{L7}^-$ to sensitize Eu(III) emission is average in the series **Eu1 - Eu7**.

It appears that the classification of the compounds **Eu1 - Eu7** into three groups based on the Judd-Ofelt parameters can be extended to include sensitizer efficiency of the ligand and the intrinsic quantum yield of the luminescent center. For the first group, the sensitizer efficiency is the highest of the entire series of complexes studied, but the intrinsic quantum yields are the lowest. The Ω_6 parameter could not be determined owing to the low intensity of the corresponding $^5D_0 \rightarrow {}^7F_6$ transition in the emission spectra. This is indicative of a relatively covalent nature of the Eu-O bonds in the complex. Because of the 4,4'-substitution pattern, both resonance and inductive effects play a role. Although the

halogens are electron-withdrawing, resonance structures that increase the electron density at the donor atoms are present. This nature is reflected in the Hammett σ constants for the halogens, which have a more chemical background [42]. Some relevant Hammett parameters are given in Table 5.4. The halogens have positive σ_p, indicating their overall electron-withdrawing nature, but negative σ_R, indicating electron donation by resonance. This electron donating resonance effect is not possible in the ligands of the second group, with the halogen on the 3-position. Hence, only the withdrawing inductive effect remains, which is indicated by the positive values for σ_m of the halogens in Table 5.4. In turn, this results in a less covalent Eu-O bond, which is reflected by increased Ω_6 parameters. The slightly increased values for the Ω_4 and the nonzero values for the Ω_6 parameters are the main differences comparing the second group to the first. It should be noted here that the slightly electron donating 4'-Me substituent is not present in **Eu5**. This might partially explain the increased Ω_2 and η_{sens} parameters in Table 5.3 for this compound. The last group, compound **Eu7**, is characterized by the lowest Ω_2 parameter and the longest radiative and experimental lifetimes of the entire series. In this compound, an electron donation by resonance of the chloride p orbitals with the aromatic system is possible. However, unfortunately no reliable σ_o parameters exist as steric effects play a major role on the ortho position.

Table 5.4: Selected Hammett σ constants, compiled from ref [42].

Substituent	σ_m	σ_p	σ_I	σ_R
CH_3	– 0.07	– 0.17	–0.04	–0.11
F	0.34	0.06	0.52	–0.34
Cl	0.37	0.23	0.47	–0.23
Br	0.39	0.23	0.44	–0.19
I	0.35	0.18	0.39	–0.16

Notes: Hammett σ parameters reflect the electron withdrawing (positive values) and electron donating (negative values) properties of substituents on a phenyl ring with respect to hydrogen. σ_m: overall σ parameter for the meta position, σ_p: overall σ parameter for the para position, $\sigma_{I/R}$: parameter describing just inductive/resonance effects.

5.5 Conclusion

Seven new Eu(III) complexes with various substituted dibenzoylmethane ligands have been synthesized in yields ranging from 46% to 100%. In addition, two new compounds of the $[Eu(dbm)_4]^-$ complex ion with NBu_4^+ and Li^+ have been prepared. Photoluminescence studies indicate that ligand-centered excitation in the near-UV spectral region results in emission from the Eu(III) center for all complexes. Analysis of the corrected emission spectra reveals the effects of the ligand substituents on the environment of the Eu(III) ion, as well as the effect on the antenna efficiency of the ligands. These effects can be at least qualitatively understood by the electron-withdrawing and donating properties of the

substituents. Substitution with F and Br on the para position gives rise to highly efficient sensitization of Eu(III) luminescence, but results in a coordination sphere around Eu(III) that gives rise to efficient non-radiative quenching. This severely limits the overall photoluminescence quantum yield of the compounds. Substitution on the meta position of the phenyl ring gives results in lower sensitizer efficiencies but higher intrinsic quantum yields of the luminescent center. In addition, there appears to be a minor improvement in sensitizer efficiency when the substituent's abilities to stabilize the ligand T*-state increases. Ortho substitution leads to important changes in the coordination environment of the Eu(III) ion, as evidenced by the intensity parameters. In addition to the substituents, the counter ion has a substantial influence on the photophysical properties of the compounds.

5.6 References

[1] J.J. Freeman and G.A. Crosby, *J. Phys. Chem.*, 67 (1963) 2717-2723.

[2] N. Filipescu, W.F. Sager, and F.A. Serafin, *J. Phys. Chem.*, 68 (1964) 3324-3346.

[3] W.F. Sager, N. Filipescu, and F.A. Serafin, *J. Phys. Chem.*, 69 (1965) 1092-1100.

[4] R.G. Charles and E.P. Riedel, *J. Inorg. Nucl. Chem.*, 28 (1966) 3005-3018.

[5] L.R. Melby and N.J. Rose, Eight coordinate trivalent rare earth metal chelates with β-diketones, Pat.no US 3254103, 1966.

[6] K. Binnemans, *Rare earth beta-diketonates*, in *Handbook on the Physics and Chemistry of Rare Earths*, 2005, Elsevier. 107-272.

[7] G.S. Hammond, W.G. Borduin, and G.A. Guter, *J. Am. Chem. Soc.*, 81 (1959) 4682-4686.

[8] W. Schwack and T. Rudolph, *J. Photochem. Photobiol., B*, 28 (1995) 229-234.

[9] J.-C. Hubaud, I. Bombarda, L. Decome, J.-C. Wallet, and E.M. Gaydou, *J. Photochem. Photobiol., B*, 92 (2008) 103-109.

[10] I. Karlsson, L. Hillerstrom, A.L. Stenfeldt, J. Martensson, and A. Borje, *Chem. Res. Toxicol.*, 22 (2009) 1881-1892.

[11] J. Zawadiak and M. Mrzyczek, *Spectrochim. Acta A*, 96 (2012) 815-819.

[12] M.L.P. Reddy, V. Divya, and R.O. Freire, *Dalton Trans.*, 40 (2011) 3257-3268.

[13] A. Mech, M. Karbowiak, C. Görller-Walrand, and R. Van Deun, *J. Alloy. Compd.*, 451 (2008) 215-219.

[14] S.M. Bruno, R.A.S. Ferreira, F.A. Almeida Paz, L.s.D. Carlos, M. Pillinger, P. Ribeiro-Claro, and I.S. Gonçalves, *Inorg. Chem.*, 48 (2009) 4882-4895.

[15] J.C. de Mello, H.F. Wittmann, and R.H. Friend, *Adv. Mater.*, 9 (1997) 230-232.

[16] T. Kottke and D. Stalke, *J. Appl. Crystallogr.*, 26 (1993) 615-619.

[17] G.M. Sheldrick, *Acta Crystallogr., Sect. A. Found. Crystallogr.*, 64 (2008) 112-122.

[18] G.M. Sheldrick, *SHELXS–97*, *Bruker AXS Inc., Madison, Wisconsin*, 1997.

[19] Nonius, *COLLECT*, *Nonius BV, Delft, The Netherlands*, 2002.

[20] L.M. Sweeting and A.L. Rheingold, *J. Am. Chem. Soc.*, 109 (1987) 2652-2658.

[21] F.A. Cotton, L.M. Daniels, and P. Huang, *Inorg. Chem. Commun.*, 4 (2001) 319-321.

[22] S. Akerboom, M.S. Meijer, M.A. Siegler, W.T. Fu, and E. Bouwman, *J. Lumin.*, 145 (2014) 278-282.

[23] A.G. Orpen, L. Brammer, F.H. Allen, O. Kennard, D.G. Watson, and R. Taylor, *J. Chem. Soc. Dalton Trans.*, (1989) S1-S83.
[24] R. Reisfeld, E. Zigansky, and M. Gaft, *Mol. Phys.*, 102 (2004) 1319 - 1330.
[25] B.R. Judd, *Phys. Rev.*, 127 (1962) 750-761.
[26] G.S. Ofelt, *J. Chem. Phys.*, 37 (1962) 511-520.
[27] J.H.S.K. Monteiro, I.O. Mazali, and F.A. Sigoli, *J. Fluoresc.*, 21 (2011) 2237-2243.
[28] H. Liang, Z. Zheng, Q. Zhang, H. Ming, B. Chen, J. Xu, and H. Zhao, *J. Mater. Res.*, 18 (2003) 1895-1899.
[29] M.H.V. Werts, R.T.F. Jukes, and J.W. Verhoeven, *Phys. Chem. Chem. Phys.*, 4 (2002) 1542-1548.
[30] C. Görller-Walrand and K. Binnemans, *Spectral intensities of f-f transitions*, in *Handbook on the Physics and Chemistry of Rare Earths*, 1998, Elsevier. 99-264.
[31] S. Tanabe, T. Ohyagi, N. Soga, and T. Hanada, *Phys. Rev. B*, 46 (1992) 3305-3310.
[32] C.K. Jørgensen and R. Reisfeld, *J. Less-common. Met.*, 93 (1983) 107-112.
[33] H. Ebendorff-Heidepriem, D. Ehrt, M. Bettinelli, and A. Speghini, *J. Non-Cryst. Solids*, 240 (1998) 66-78.
[34] M.P. Hehlen, M.G. Brik, and K.W. Krämer, *J. Lumin.*, 136 (2013) 221-239.
[35] S. Tanabe, K. Takahara, M. Takahashi, and Y. Kawamoto, *J. Opt. Soc. Am. B*, 12 (1995) 786-793.
[36] M.H.V. Werts, *Sci. Prog.*, 88 (2005) 101-131.
[37] J.-C.G. Bünzli, *Chem. Rev.*, 110 (2010) 2729-2755.
[38] L. Armelao, S. Quici, F. Barigelletti, G. Accorsi, G. Bottaro, M. Cavazzini, and E. Tondello, *Coord. Chem. Rev.*, 254 (2010) 487-505.
[39] B. Francis, D.B.A. Raj, and M.L.P. Reddy, *Dalton Trans.*, 39 (2010) 8084-8092.
[40] S. Faulkner, S.J.A. Pope, and B.P. Burton-Pye, *Appl. Spectrosc. Rev.*, 40 (2005) 1-31.
[41] M. Latva, H. Takalo, V.M. Mukkala, C. Matachescu, J.C. Rodriguez-Ubis, and J. Kankare, *J. Lumin.*, 75 (1997) 149-169.
[42] M. Montalti, A. Credi, L. Prodi, and M.T. Gandolfi, *Handbook of Photochemistry 3rd edition*, 2006, Boca Raton, Florida: CRC Press.